Colloid and Interface Science Communications 33 (2019) 100219

Contents lists available at ScienceDirect

Colloid and Interface Science Communications

journal homepage: www.elsevier.com/locate/colcom

Gold nanoparticles deposited on silica microparticles - Electrokinetic characteristics and application in SERS

Dawid Lupa[a,*], Magdalena Oćwieja[a], Natalia Piergies[b], Andrzej Baliś[c], Czesława Paluszkiewicz[b], Zbigniew Adamczyk[a]

[a] Jerzy Haber Institute of Catalysis and Surface Chemistry, Polish Academy of Sciences, Niezapominajek 8, PL-30239 Krakow, Poland
[b] Insitute of Nuclear Physics Polish Academy of Sciences, PL-31342 Krakow, Poland
[c] Faculty of Chemistry, Jagiellonian University, Gronostajowa 2, PL-30387 Krakow, Poland

ARTICLE INFO

Keywords:
Gold nanoparticles
Nanoparticle immobilization
SERS
Particle characterization
Particle engineering

ABSTRACT

The range of applicability of nanoparticle aggregates in surface enhanced Raman spectroscopy (SERS) sensing is limited. Therefore, in this work, an alternative route is developed consisting in a deposition of positively charged gold nanoparticles on silica carrier microparticles in an electrostatic interaction driven colloidal self-assembly process. The obtained composite particles of a raspberry structure and controlled gold nanoparticle coverage are utilized as SERS substrates in the sensing of rhodamine B. It is shown that the composites show significantly larger enhancement efficiency compared to gold nanoparticle aggregates produced in a conventional way. This effect was attributed to the adsorption of rhodamine B molecules at an available silica particle surface in the vicinity of immobilized gold nanoparticles. The results obtained in this work show that nanoparticle immobilization may be an efficient strategy to increase SERS sensing efficiency.

1. Introduction

As shown in some works [1–3], the use of gold nanoparticles (AuNPs) as SERS substrates requires a surface cleaning from adsorbed stabilizers which may result in particle aggregation. This can significantly influence the optical properties of nanoparticles by affecting the maximum of localized surface plasmon resonance (LSPR) band [4,5] or even may result in loss of their plasmonic properties [6]. On the other hand, the aggregation process produces localized electromagnetic field regions (hot-spots), which are responsible for an additional enhancement effect [7–10]. Nevertheless, due to the variability of aggregation process [11] the reproducibility of the enhancement factor (EF) is rather low. Therefore one can expect that the use of AuNPs aggregates in real SERS analyses is limited [12]. For this reason, new reproducible strategies for the generation of hot-spots in SERS substrates are still needed.

Another example of an approach utilized for the hot-spot generation is immobilization of AuNPs at various solid supports, especially the surface of colloidal carriers. Except for the hot-spot generation, one can also expect that AuNP immobilization may result in the increase in their stability. As shown in previous work [13], compared to native suspension, AuNPs immobilized at polystyrene microparticles are more resistant to pH changes. So far, AuNP composites with polymer particles [14–16], polyelectrolyte modified particles [17,18] and various oxide particles [19–21] were successfully obtained and applied as SERS substrates.

Among a variety of particles which can be used to immobilize AuNPs, due to their mechanical stability, chemical inertia and biodegradability [22] silica particles (SiO_2Ps) are especially attractive. Moreover, the coating of SiO_2Ps with AuNPs results in a distinct change in the dielectric constant at phase boundary and in the electron share phenomenon [23]. For this reason, various synthetic procedures for the preparation of such particles, including chemical linking of AuNPs with SiO_2Ps [24], immobilization of AuNPs on SiO_2Ps [25,26] and chemical reduction of gold ion precursors [27], were recently developed.

Oldenburg et al. [28] reported a synthetic procedure for the preparation of core-shell, raspberry-like nanostructures with tunable optical resonance profile. SiO_2Ps of two different sizes (75 nm and 170 nm) were used as core materials while the shell of AuNPs (18 nm - 30 nm) was formed in a seed growth process. It was shown that the increase in the core/shell thickness ratio resulted in a red-shift of resonance wavelength. However, when a uniform gold layer was formed, backward blue-shift in optical resonance frequency was observed. This finding indicates that the structure of the AuNPs@SiO_2Ps SERS

* Corresponding author.
E-mail address: nclupa@cyf-kr.edu.pl (D. Lupa).

https://doi.org/10.1016/j.colcom.2019.100219
Received 2 September 2019; Received in revised form 9 October 2019; Accepted 29 October 2019
Available online 08 November 2019

substrate (uniform layer or nanoparticle monolayer) is a crucial factor determining its optical properties. However, the electrokinetic properties of obtained particles were not determined.

Raspberry-like particles composed of silica core and AuNP shell were also studied by Sadtler et al. [29]. In their approach, SiO_2Ps (330–550 nm in diameter) were functionalized by adsorption of polyethylenimine in order to provide a positive surface charge. Afterward, negatively charged citrate-stabilized AuNPs (20; 30; 40; and 80 nm in diameter) were deposited at SiO_2Ps in colloidal self-assembly process. Then, the influence of the coverage of the shell layer of AuNPs on optical properties of obtained composites was determined using UV–Vis spectroscopy. It was confirmed that compared to the native suspension of AuNPs, their composites with SiO_2 exhibited slight red-shift (from 520 nm to 540 nm) of the plasmon band. The shift in LSPR peak increased with AuNPs surface coverage. This effect was attributed to electromagnetic coupling phenomenon between AuNPs in monolayer.

In the work of Khurana et al. [30], SiO_2Ps (average size of 800 nm), were modified by adsorption of (3-aminopropyl)triethoxysilane and used as a supporting material for the formation of shells composed of negatively charged AuNPs. The composites were used as substrates for SERS investigations of crystal violet (CV) and single wall carbon nanotubes (SWNT). Analysis of the spectra confirmed the applicability of the composites as SERS substrates. The enhancement factor varied between 3.2×10^7 and 1.42×10^8 in the case of CV and SWNT, respectively. However, the coverage of AuNP layer was not quantitatively determined.

A detailed study of AuNP@SiO_2Ps raspberry-like composites was performed by Beulze et al. [26] who investigated the influence of shell roughness on optical properties and enhancement factor of the SERS signals of tiophenol. In this case, negatively-charged AuNPs of five various diameters (10; 20; 30; 40 and 50 nm) were deposited on PDADMAC modified SiO_2Ps (100 nm in diameter). This allowed to obtain a series of AuNPs@SiO_2Ps composites having various AuNPs to SiO_2Ps diameter ratio. Analyzing the extinction spectra of the composites it was found that red-shift of LSPR band is dependent on the diameter ratio of the particles. In the case of 30 nm AuNPs, the LSPR red-shift was equal to 10 nm whereas the use of 10 nm AuNPs resulted in 70 nm LSPR shift. It is worth mentioning that this considerable shift may result from quantum confining effect which is only characteristic for nanoparticles of diameter equal to 10 nm or less. Surprisingly, those results were in disagreement with the SERS activity measurements which showed that tiophenol spectra intensity increases with AuNPs size. Despite the fact that AuNP coverage was roughly estimated, no data about electrokinetic properties was reported.

Analysis of literature data confirms the importance of hybrid microparticles composed of AuNPs shell and silica core in modern SERS sensing. It is clearly visible that attention of the researchers is focused mainly on analytical aspects of particles, whereas other important factors such as electrokinetic properties and stability of obtained systems are rather overlooked.

Therefore, in this work a facile procedure for the preparation of AuNPs@SiO_2Ps of a controlled morphology, coverage, electrokinetic properties and potential utility as SERS substrates is developed. Due to the biodegradability of SiO_2Ps and biocompatibility of AuNPs, the composites could be used for in-vivo analyzes. In contrast to previous literature reports, the influence of surface coverage and overall SERS substrate concentration on EF and enhancing efficiency per single AuNP is determined and discussed.

2. Materials and methods

2.1. Chemicals

Tetraethoxysilane (TEOS), tetrachloroauric(III) acid trihydrate ($HAuCl_4 \cdot 3H_2O$), sodium borohydride ($NaBH_4$), cysteamine hydrochloride ($HSCH_2CH_2NH_2 \cdot HCl$), sodium chloride, hydrochloric acid, sodium hydroxide and rhodamine B (RB) are supplied by Sigma-Aldrich. Ammonia solution (30%, p.a.) and ethanol (96%, p.a.) were products of Chempur (Piekary Slaskie, Poland). All chemicals were used as received. Aqueous solutions used in the studies are prepared using ultrapure water obtained from the Milli-Q Elix& Simplicity 185 purification system (Millipore SA Molsheim, France). The ultrapure water conductivity was 0.06 μS cm^{-1}.

2.2. Synthesis of particles

Silica particles were synthesized using modified Stöber method [31]. Briefly, 100 mL of ethanol, 8 mL of deionized water, and 4 mL of ammonia solution were mixed and kept at 15 °C. Subsequently, 6 mL of TEOS was added to the mixture, that was stirred for 6 h at the same temperature leading to the formation of suspension of SiO_2Ps. Then, this solution was centrifuged (5 min, 7900 RCF) and the particles were washed with ethanol and dried at 50 °C overnight.

Gold nanoparticles were synthesized using sodium borohydride and cysteamine hydrochloride [32,33]. Firstly, 20 mL of freshly prepared aqueous solution of sodium borohydride (10 mM) was added dropwise to 120 mL of 1.42 mM tetrachlorauric(III) acid. After 10 min of stirring of suspension, 1.5 mL of 213 mM solution of cysteamine hydrochloride was added to the reaction mixture. The stirring was continued over 30 min. Then, the suspension was purified according to procedure described previously [33].

2.3. Preparation of AuNPs@SiO_2Ps composites

Ionic strength and the concentration of purified AuNP suspension were adjusted by adding a proper volume of ultrapure water and 0.1 M NaCl, respectively. In this way, a set of AuNP suspensions of controlled concentrations and ionic strength (10^{-3} M and 3×10^{-3} M) was obtained. This procedure was also applied in order to obtain the suspensions of SiO_2Ps of desired concentration and ionic strength. Afterward, the suspensions of SiO_2Ps and AuNPs of the same ionic strength were mixed together for 20–30 min. In this way, 10 mL of the mixture containing a constant concentration of the SiO_2Ps equal to 50 mg L^{-1} or 100 mg L^{-1} and various content of the AuNPs was obtained. As previously discussed, this period of time was adequate in order to efficiently immobilize AuNPs on the SiO_2Ps [13].

2.4. Determination of physicochemical properties of particles

The mass concentration of the stock suspensions of SiO_2Ps and AuNPs was determined using two different methods: gravimetric analysis and suspension density measurements. In the first approach, SiO_2Ps concentration was calculated based on sample mass changes upon drying. In the second case, the density of SiO_2Ps suspension and its effluent was determined by high-precision DMA5000M densitometer (Anton Paar) and the concentration was determined based on the suspension, effluent and amorphous silica density. The formula allowing the calculation of particle mass concentration can be found in previous work [33].

The morphology and the size distribution of SiO_2Ps, AuNPs and AuNPs@SiO_2Ps were derived from micrographs acquired using JEOL JSM-7500F Field Emission scanning electron microscope (SEM). The surface concentration of the AuNPs deposited on the SiO_2Ps were determined according to the methodologies described in previous work [13].

The size distribution and the stability of SiO_2Ps, AuNPs and AuNPs@SiO_2Ps dispersed in the suspensions of controlled ionic strength (I) were determined applying the dynamic light scattering (DLS) using Zetasizer Nano ZS instrument. The particle diffusion coefficients (D) were converted to the hydrodynamic diameter (d_H) using the Stokes-Einstein relationship [13]. The same apparatus was applied to determine electrophoretic mobility (μ_e) of the SiO_2Ps, AuNPs and

AuNPs@SiO_2Ps exploiting the laser Doppler velocimetry (LDV) technique.

2.5. Measurements of RB spectra in the presence of AuNPs and AuNPs@SiO_2Ps

Raman spectra of rhodamine B (RB) in aqueous solutions of controlled concentrations (from 5×10^{-5} M to 4.75×10^{-4} M) were recorded in the presence of the AuNPs and the AuNPs@SiO_2Ps. The surface enhanced Raman spectra (SERS) were measured in the AuNP suspension of a concentration equal to 50 mg L^{-1}. For suspensions of the AuNPs@SiO_2Ps, the concentration of the SiO_2Ps ranged from 20 to 50 mg L^{-1} and the coverage of deposited AuNPs monolayers changed from 0.01 to 0.23. The samples for such investigations were prepared by dispersing freshly centrifuged AuNPs@SiO_2Ps in a proper volume of RB solution. After incubation time equal to 30 min, particles were centrifuged, washed with ultrapure water and redispersed. For comparison, spectra of RB in its aqueous solution and in the presence of SiO_2Ps and AuNPs were also recorded.

The spectra were obtained using a Renishaw InVia Raman spectrometer equipped with an optical confocal microscope, a diode laser emitting at 785 nm, and a CCD detector. The dry LeicaN PLAN EPI (20×, NA 0.4) objective was used. The power of the laser at the sample position was ca. 30 mW for a measurement. One scan with the integration time of 60 s was enough to obtain good signal/noise ratio. The spectrometer was calibrated using the Raman scattering line generated by an internal silicon plate. The drop of appropriate suspension or RB solution was placed on microscope slides and a laser spot was focused inside the drop. For all spectra, a multipoint baseline correction (five points) was applied.

3. Results and discussion

3.1. Characteristics of particles

Typical SEM micrographs and histograms obtained by their analysis are shown in Fig. 1. One can see that SiO_2Ps are spherical and monodisperse, whereas AuNPs are mostly spherical and their polydispersity is slightly larger. Analyzing the histograms, it is determined that the average size of SiO_2Ps and AuNPs was equal to 605 ± 40 nm and 12 ± 3 nm, respectively. These values correspond to the polydispersity index (PDI) value equal to 0.07 and 0.25 for SiO_2Ps and AuNPs, respectively.

Next, the diffusion coefficients and electrophoretic mobilities of the particles were measured for a broad range of ionic strength using DLS and LDV methods. These results are collected in Table 1 and presented in Fig. 2 as the dependence of the hydrodynamic diameter and the zeta potential of particles on ionic strength. As seen, the hydrodynamic diameter of AuNPs is equal to 12 nm for ionic strength up to 3×10^{-3} M. For larger ionic strength, an abrupt increase in the hydrodynamic diameter of AuNPs is observed. This effect is attributed to the aggregation of the AuNPs caused by decrease in interparticle electrostatic repulsion energy. In contrast, the hydrodynamic diameter of SiO_2Ps was equal to 640 nm for the whole ionic strength range. This suggests that the SiO_2Ps are stable under such conditions (at pH 6.2).

The dependence of the zeta potential of the AuNPs and the SiO_2Ps on ionic strength is presented in Fig. 2b. As seen, the zeta potential of AuNPs decreases monotonically from 44 mV to 30 mV while ionic strength increases from 10^{-4} M to 3×10^{-3} M. On the other hand, the zeta potential of SiO_2Ps increased from −60 mV to −34 mV for an analogous change in ionic strength. This can be attributed to the decrease in the double layer thickness which implies the decrease in both Henry's function and zeta potential value.

As mentioned before, the size of SiO_2Ps determined from the SEM analysis was equal to 605 ± 40 nm. This is slightly smaller than the diameter derived from the DLS measurements (Fig. 2a). This difference is in accordance to the measurements performed by Barahona et al. [34].

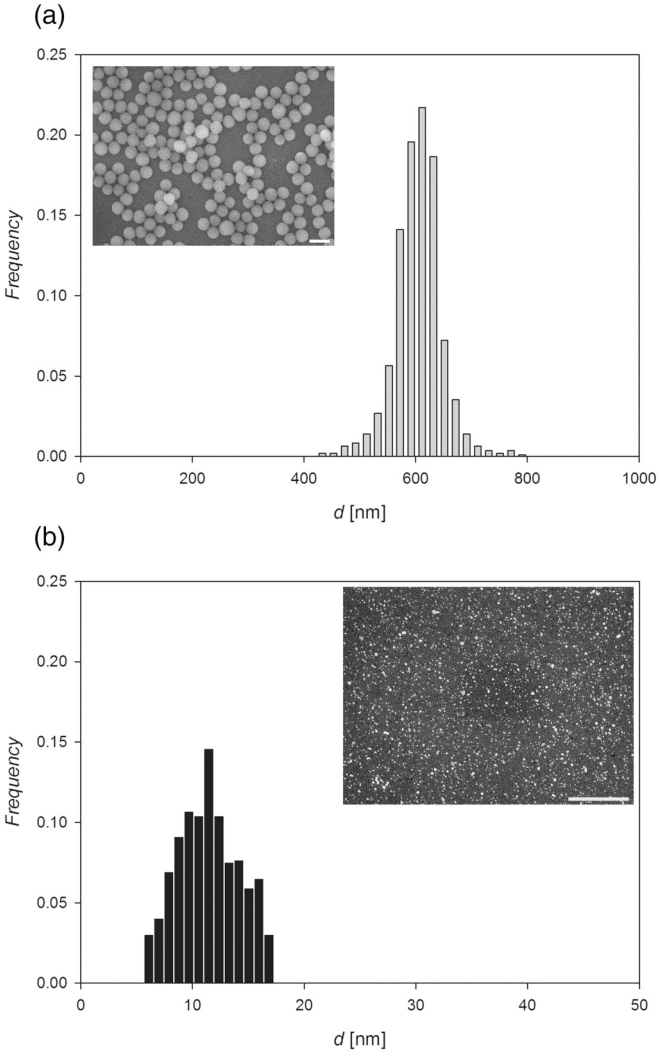

Fig. 1. Size distribution of (a) SiO_2Ps and (b) AuNPs derived from SEM. Scale bar length is equal to 1 μm.

3.2. Formation and properties of AuNPs@SiO_2Ps composites

The formation of AuNPs@SiO_2Ps was studied using electrophoretic mobility measurements and SEM imaging. In the former case, the zeta potential of AuNPs@SiO_2Ps was calculated using Henry's formula. The dependencies of zeta potential of the AuNPs@SiO_2Ps on the AuNPs concentration are shown in Fig. 3. (the upper horizontal axis). It is also useful to express these dependencies using nominal coverage of the AuNP at SiO_2Ps (θ_{AuNPs}), which can be calculated from the following formula:

$$\theta_{AuNPs} = \frac{1}{4} \frac{\rho_{SiO_2Ps} d_{SiO_2Ps}}{\rho_{Au} d_{AuNPs}} \frac{c_{AuNPs}}{c_{SiO_2Ps}} \quad (1)$$

where d_{AuNP} is the hydrodynamic diameter of AuNPs, $c_{AuNPs}$is the bulk concentration of AuNPs and ρ_{Au} is the density of gold in bulk.

Defining θ_{AuNPs} one can express the experimental results as the dependence of AuNPs@SiO_2Ps zeta potential on the nominal coverage of AuNPs. As shown in Fig. 3, an abrupt increase in the AuNPs@SiO_2Ps

Table 1
Selected physicochemical properties of the SiO_2Ps and AuNPs.

	Property [unit], symbol		
Particles, values	SiO_2Ps	AuNPs	Remarks
Density [g cm^{-3}], ρ_p	1.85	19.3	Experimental studies (SiO_2Ps) and literature data [15] (AuNPs)
Particle diameter [nm]	605 ± 40	12 ± 3	From SEM
Diffusion coefficient [cm^2 s^{-1}], D	7.64×10^{-9}	5.22×10^{-7}	from DLS, pH 6.2, T = 25 °C, $I = 3 \times 10^{-3}$ M
Hydrodynamic diameter [nm], d_H	640 ± 13	12 ± 3	Calculated from the Stokes-Einstein relationship, pH 6.2, T = 25 °C,$I = 3 \times 10^{-3}$ M
Geometrical cross-section area [nm^2], S_g	1.03×10^5	69.4	From geometry
Particle surface area [nm^2], S	4.12×10^5	277	From geometry
Electrophoretic mobility [(μmcm)(Vs)$^{-1}$], μ_e			pH 6.2, T = 25 °C,
	−4.70 ± 0.18	2.33 ± 0.12	$I = 10^{-4}$ M
	−3.37 ± 0.11	1.86 ± 0.21	$I = 10^{-3}$ M
	−2.66 ± 0.15	1.59 ± 0.19	$I = 3 \times 10^{-3}$ M
Zeta potential [mV], ζ			Calculated from the Henry's model, for pH 6.2, T = 25 °C,
	−60 ± 2	44 ± 2	$I = 10^{-4}$ M
	−43 ± 1	35 ± 4	$I = 10^{-3}$ M
	−34 ± 2	30 ± 4	$I = 3 \times 10^{-3}$ M

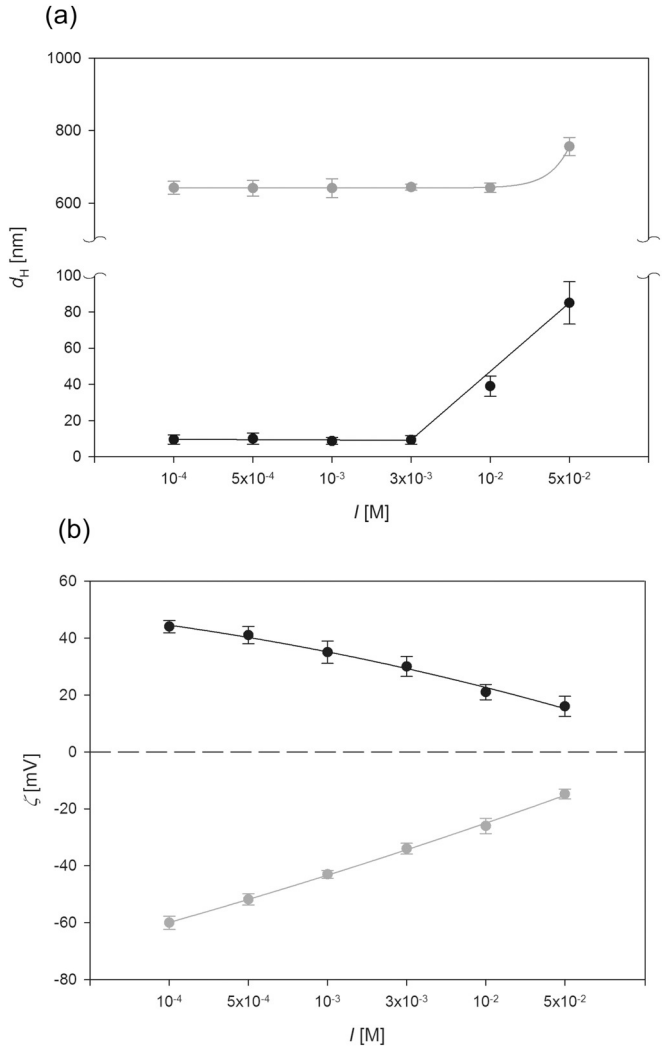

Fig. 2. Dependence of (a) hydrodynamic diameter and (b) zeta potential of: (●) SiO_2Ps and (●) AuNPs on ionic strength. Measurements conditions: c_{AuNPs} = 20 mg L^{-1};c_{SiO_2Ps} = 50 mg L^{-1}, pH 6.2. The solid lines represent fits of experimental results.

zeta potential with AuNP coverage is observed. This leads to the inversion of the zeta potential sign which occurs for AuNPs coverage exceeding 0.1. This observation agrees with previous results [13] obtained for AuNPs monolayers deposited on of poly(styrene) particles. For larger AuNPs coverage, a limiting zeta potential was attained. It was equal to 26 mV and 22 mV for the ionic strength equal to 10^{-3} and 3×10^{-3} M, respectively.

The experimental results presented in Fig. 3 are interpreted in terms of the electrokinetic 3D model described in details elsewhere [35]. The results obtained using this model are plotted as solid lines. As seen, the agreement between experimental data and theoretically predicted dependence is satisfactory. AuNPs coverage was also determined using SEM. Micrographs of AuNPs@SiO_2Ps with different surface coverage were shown as insets in Fig. 3. As the AuNPs are mostly deposited as isolated entities, it is possible to evaluate their coverage (θ_{AuNPs}) using direct enumeration procedure. It is determined that jamming coverage of AuNPs is equal to 0.23 and 0.28 for the ionic strength equal to 10^{-3} and 3×10^{-3}, respectively. These results agree with the results obtained using electrokinetic measurements. This confirms the applicability of the in situ electrokinetic measurements for determination of nanoparticle coverage at microparticle surface. Taking into the account that colloidal stability of obtained particles is crucial factor determining their utility in analyzes, their stability was also evaluated. In result, no significant changes in the hydrodynamic diameter or zeta potential were observed for 12 h of storage.

3.3. Spectroscopic detection of RB in the presence of AuNPs

The AuNPs in the native suspensions and the AuNPs@SiO_2Ps of a controlled monolayer coverage were investigated as SERS substrates for RB detection. Firstly, spectra of pure RB solutions of various concentrations were recorded. The results obtained for RB solutions of the concentrations 10^{-5} M, 10^{-4} M and 4.7×10^{-4} M. are shown in Fig. 4. Additionally, the SERS spectrum of RB of the concentration of 4.7×10^{-4} M recorded in the presence of the AuNPs of the concentration of 50 mg L^{-1} at ionic strength 7×10^{-3} M is presented. It is worth mentioning that the AuNPs were unstable at applied ionic strength (Fig. 2a). One can therefore expect that under such conditions AuNP aggregates can be formed. This allowed to generate more hot-spots and to create suitable conditions for detection of RB.

Analyzing the results presented in Fig. 4 one can notice that the spectral pattern of RB indicates that the concentration of 4.7×10^{-4} M

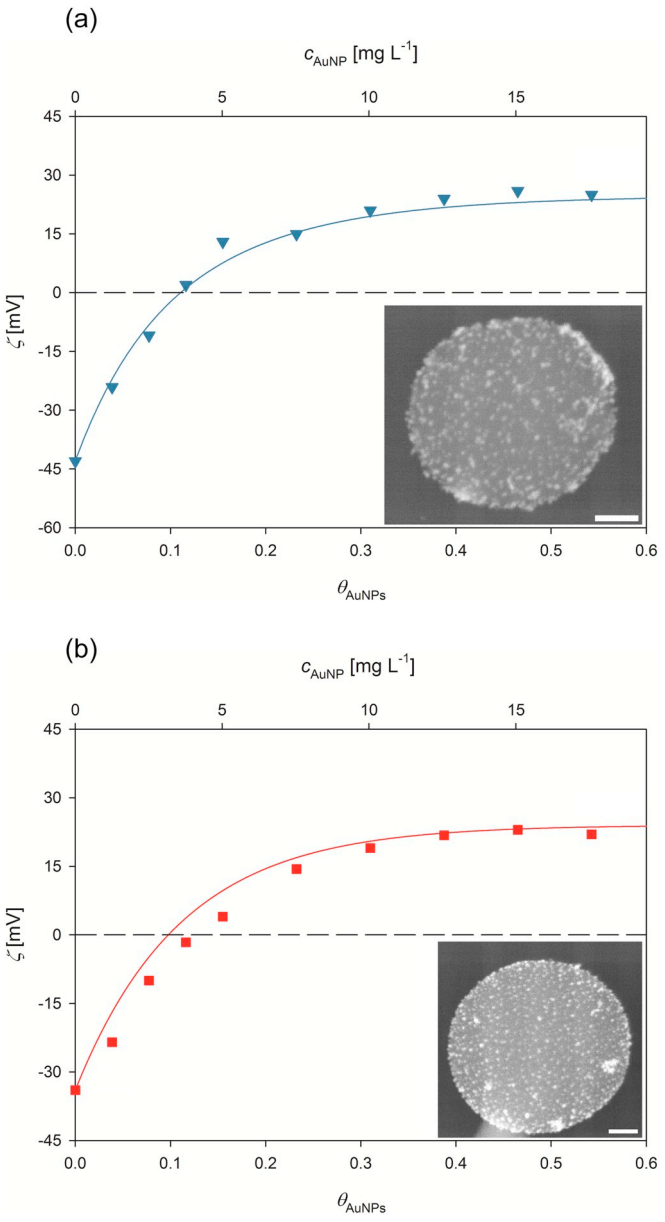

Fig. 3. Dependence of the zeta potential of the SiO_2Ps on the AuNP concentration in the suspension (the upper horizontal axis) and the nominal coverage of AuNPs on the SiO_2Ps (the lower horizontal axis). Deposition conditions: c_{SiO_2Ps} = 50 mg L^{-1}, T = 25 °C, pH 6.2, ionic strength: (a) 10^{-3} M and (b) 3×10^{-3} M. The solid lines denote theoretical results calculated from the electrokinetic 3D model. The insets show AuNPs@SiO_2Ps of different coverage: (a) 0.13, (b) 0.25. The scale bar corresponds to 100 nm.

is needed to obtain reasonable signal to noise ratio. However, as seen in Fig. 4 the application of the AuNPs as a SERS active substrate increases the detected spectral signal. The intensity of the 1511 cm^{-1} band was employed for calculation of enhancement factor (EF), which is calculated using the following formula [36]:

$$EF = \frac{I_{SERS} c_{Raman}}{I_{Raman} c_{SERS}} \quad (2)$$

where: I_{SERS} is the intensity of the SERS band at 1511 cm^{-1}; I_{Raman} is the intensity of the corresponding band in the Raman spectrum; c_{Raman} is the concentration of RB in the solution without the AuNPs and c_{SERS} is the concentration of RB in the suspension of the AuNPs.

From Eq. (2) it was found that EF is equal to 1.92. This value is rather low compared to literature data [30]. Nevertheless, it was shown

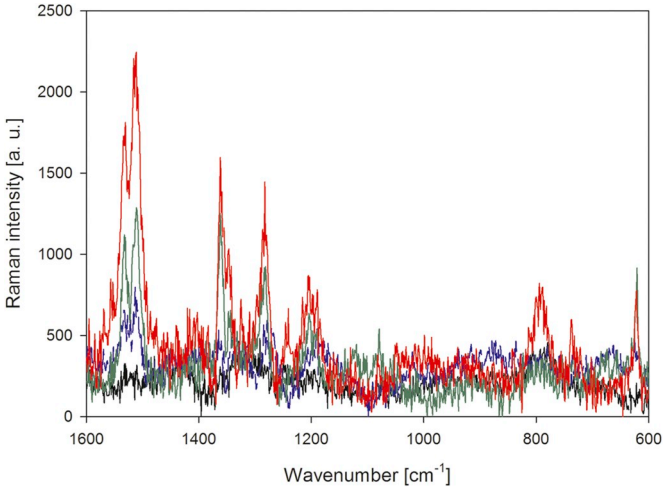

Fig. 4. (−) SERS spectrum of RB of the concentration equal to 4.7×10^{-4} M recorded in the presence of the AuNPs (50 mg L^{-1}) at ionic strength of 7×10^{-3} M and the Raman spectra of RB recorded for its aqueous solutions of the concentration equal to: (—) 10^{-5} M, (—) 10^{-4} M and (—) 4.7×10^{-4} M.

that negatively charged AuNPs provide larger EF compared to those with positive charge [37]. For AuNPs, which are stabilized by cysteamine moieties, one can suspect that the availability of the nanoparticle surface is lowered. This causes less effective analyte adsorption on AuNPs surface.

On the other hand, as confirmed by Ruan [38], there can be another mechanism responsible for enhancement effect. In aforementioned work, the AuNPs aggregates were used as SERS substrates for the detection of perchlorate. It was suggested that strong a electrostatic attraction between perchlorate and amine groups enabled a close contact of analyte and AuNP surface and hence enhanced the Raman signal. This hypothesis was verified by performing additional SERS measurements at pH of 12. In this case, no enhancement of Raman signal was observed [38]. This important finding indicates that electrostatic interactions between the stabilizer and the analyte may be sufficient for the enhancement effect whereas the analyte adsorption on AuNPs surface is not necessary.

One can expect that due to the size and structure of RB molecule, its electrostatic binding to protonated amine groups is rather impossible. Because the pK_a of RB is equal to 3.1 [39] one can calculate that such molecule is fully ionized at pH 6.2. Bearing in mind that the dissociation of RB molecule creates a formal negative charge at carboxyl group, it is expected that RB could easily bind to cysteamine moieties present at AuNPs surface.

3.4. Spectroscopic detection of RB in the presence of AuNPs@SiO_2Ps

Because the AuNPs gave relatively little enhancement of the SERS signal, the usefulness of the AuNPs@SiO_2Ps for the RB detection was investigated. Initially, the influence of the AuNPs coverage on the enhancement effect at RB concentration of 4.7×10^{-4} M was evaluated. The experiments were carried out for the AuNPs@SiO_2Ps concentration equal to 50 mg L^{-1} (in reference to SiO_2Ps) at ionic strength of 7×10^{-3} M. The bulk conditions which were applied in the experiments utilizing pure suspensions of AuNPs were matched analogously. In contrast to previous studies, the AuNPs were deposited on the SiO_2Ps in electrostatic-driven immobilization process and formed well-defined monolayers of coverage of 0.05, 0.10 and 0.23. The SERS spectra of RB recorded under these conditions are presented in Fig. 5 As seen, the increase in the AuNPs coverage induces noticeable increase in the intensity of bands stemming from RB. The EF calculated for these substrates was equal to 2.75, 3.92, and 5.75 for the AuNPs coverage of 0.05, 0.10 and 0.23, respectively. These values are rather low compared

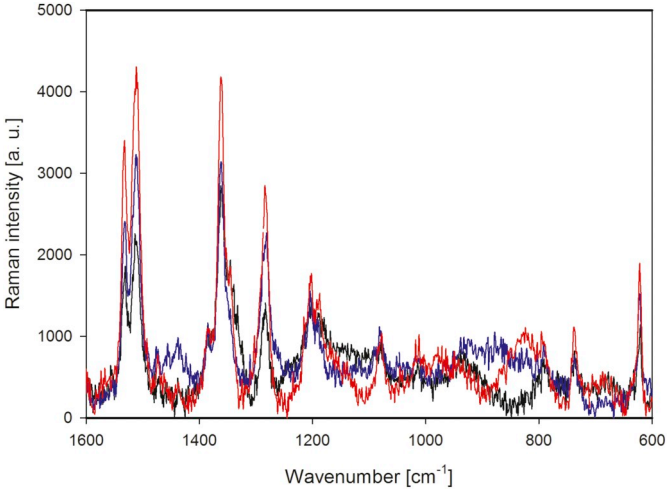

Fig. 5. The SERS spectra of RB at concentration 4.7×10^{-5} M recorded in the suspensions of AuNPs@SiO_2Ps of concentration equal to 50 mg L^{-1} ionic strength 7×10^{-3} M and the AuNP coverage equal to: (−) 0.05, (—) 0.10 and (—) 0.23.

to those obtained by Khurana (3.2×10^7) [30] and Castillo (2.3×10^4) [40] for negatively-charged AuNPs immobilized on the positively-charged SiO_2Ps. On the other hand, obtained results are comparable with those reported by Wang [41] for Au-SiO_2 composites utilized for detection of rhodamine 6G.

The comparison between result obtained for the AuNPs aggregates and AuNPs@SiO_2Ps indicate that the immobilization of the positively-charged AuNPs on the negatively-charged SiO_2Ps surface is efficient strategy which allows to increase the EF value. Moreover, due to the lateral interactions between the AuNPs deposited on the SiO_2Ps surface, the reproducibility of substrates is much larger than in the case of AuNPs aggregates. It should be mentioned that the total AuNPs concentration in the experiment performed with the use of the AuNPs@SiO_2Ps was significantly lower than in the case of the AuNPs aggregates. Using Eq. (1) one can calculate that AuNPs concentration was equal to 1.6 mg L^{-1}, 3.2 mg L^{-1} and 7.4 mg L^{-1} for the coverage equal to 0.05, 0.10 and 0.23, respectively. One can easily show that in the case of AuNPs@SiO_2Ps the enhancing efficiency per single AuNP was 20 (for $\theta_{AuNPs} = 0.23$) to 44-fold (for $\theta_{AuNPs} = 0.05$) larger. This may result from the differences in availability of the AuNPs surface which is

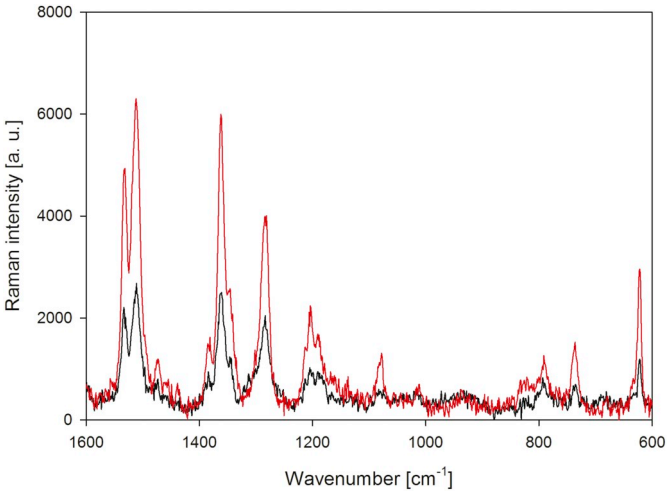

Fig. 6. The SERS spectra of RB at concentration 4.7×10^{-5} M recorded in the suspensions of AuNPs@SiO_2Ps of concentration equal to (−) 20 mg L^{-1} and (—) 50 mg L^{-1} (in reference to SiO_2Ps) at ionic strength of 7×10^{-3} M and the AuNP coverage of 0.20.

considerably lower for the AuNPs aggregates. It should be pointed out that the adsorption of RB molecules on SiO_2Ps was recently observed [42,43]. Therefore, one can expect that RB molecules adsorbs on the unoccupied SiO_2Ps surface of the AuNPs@SiO_2Ps. These RB molecules which are in the vicinity of the deposited AuNPs are prone to the field enhancement effect.

Additional measurement were performed to prove that the increase in the SERS signal intensity by the AuNPs@SiO_2Ps originates from surface plasmon enhancement of the AuNPs rather than from adsorption of RB on a bare SiO_2Ps surface. In this case, SERS spectra of RB were recorded using a native SiO_2Ps suspension of the same ionic strength, pH and RB concentration as for the AuNPs@SiO_2Ps. Under such experimental conditions, no enhancement effect was observed.

In the last part of investigation, the SERS spectra of RB were recorded for two different concentrations of the AuNPs@SiO_2Ps, namely 20 mg L^{-1} and 50 mg L^{-1} (in respect to the SiO_2Ps). In both cases, the coverage of AuNP monolayers deposited on the SiO_2Ps was equal to 0.20. The obtained results are presented in Fig. 6. As expected, the EF increased with the AuNPs@SiO_2Ps concentration and was equal to 2.11 and 5.75 for the AuNPs@SiO_2Ps concentration of 20 mg L^{-1} and 50 mg L^{-1}, respectively. Knowing the aforementioned EF values, one can calculate that their ratio is equal to 2.7, which agrees with the concentration ratio. This observation also confirms the preferential adsorption of RB molecules on the SiO_2Ps surface.

4. Conclusions

An efficient procedure for the immobilization of positively charged gold nanoparticles (AuNPs) on silica particles in a self-assembly process was developed. The progress of the monolayer formation was followed in situ measuring the electrophoretic mobility of the composite particles. The coverage was quantitatively determined using the electrokinetic model, whose utility was confirmed by a direct SEM imaging of deposited nanoparticles.

The applicability of the composites for the SERS analysis was investigated using rhodamine B as a model analyte. It was shown that increase in AuNP monolayer coverage is the most important factor affecting the enhancement efficiency.

A comparison of native AuNP and SiO_2Ps suspensions with the new composites proved a large efficiency of the latter in enhancing of the SERS signal. This effect was attributed to the plasmonic electric field exerted on the rhodamine B molecules adsorbed in the vicinity of gold particles immobilized on the silica particles.

These results suggest that instead of using aggregated nanoparticles as SERS substrate one can simply increase the sensing efficiency by immobilizing such nanoparticles on properly selected colloidal carriers. Therefore, complex particles obtained using this methodology may be a valuable starting point for new generation of SERS substrates.

Declaration of Competing Interest

The authors declare no conflict of interest.

Acknowledgements

This research was funded in part by the statutory research fund of ICSC PAS. This work was financially supported by the National Science Center under the Opus ProjectUMO-2015/19/B/ST5/00847. The SERS investigations were performed using equipment purchased in the frame of the project co-funded by the Malopolska Regional Operational Programme Measure 5.1 Krakow Metropolitan Area as an important hub of the European Research Area for 2007- 2013, project No. MRPO.05.01.00-12-013/15. The authors are grateful to Dr. Dorota Duraczyńska for imaging of the samples using scanning electron microscopy.

References

[1] V. Chegel, O. Rachkov, A. Lopatynskyi, S. Ishihara, I. Yanchuk, Y. Nemoto, J.P. Hill, K. Ariga, Gold nanoparticles aggregation: drastic effect of cooperative functionalities in a single molecular conjugate, J. Phys. Chem. C 116 (2012) 2683–2690, https://doi.org/10.1021/jp209251y.

[2] I. Blakey, Z. Merican, K.J. Thurecht, A method for controlling the aggregation of gold nanoparticles: tuning of optical and spectroscopic properties, Langmuir. 29 (2013) 8266–8274, https://doi.org/10.1021/la401361u.

[3] L. Guo, J.A. Jackman, H.H. Yang, P. Chen, N.J. Cho, D.H. Kim, Strategies for enhancing the sensitivity of plasmonic nanosensors, Nano Today 10 (2015) 213–239, https://doi.org/10.1016/j.nantod.2015.02.007.

[4] Y. Yang, S. Matsubara, M. Nogami, J. Shi, Controlling the aggregation behavior of gold nanoparticles, Mater. Sci. Eng. B Solid-State Mater. Adv. Technol. 140 (2007) 172–176, https://doi.org/10.1016/j.mseb.2007.03.021.

[5] I. Freitag, U. Neugebauer, A. Csaki, W. Fritzsche, C. Krafft, J. Popp, Preparation and characterization of multicore SERS labels by controlled aggregation of gold nanoparticles, Vib. Spectrosc. 60 (2012) 79–84, https://doi.org/10.1016/j.vibspec.2012.02.013.

[6] G. Wang, W. Sun, Optical limiting of gold nanoparticle aggregates induced by electrolytes, J. Phys. Chem. B 110 (2006) 20901–20905, https://doi.org/10.1021/jp0638843.

[7] S. Picciolini, N. Castagnetti, R. Vanna, D. Mehn, M. Bedoni, F. Gramatica, M. Villani, D. Calestani, M. Pavesi, L. Lazzarini, A. Zappettini, C. Morasso, Branched gold nanoparticles on ZnO 3D architecture as biomedical SERS sensors, RSC Adv. 5 (2015) 93644–93651, https://doi.org/10.1039/c5ra13280k.

[8] G. Yang, J. Nanda, B. Wang, G. Chen, D.T. Hallinan, Self-assembly of large gold nanoparticles for surface-enhanced Raman spectroscopy, ACS Appl. Mater. Interfaces 9 (2017) 13457–13470, https://doi.org/10.1021/acsami.7b01121.

[9] A.M. Schwartzberg, C.D. Grant, A. Wolcott, C.E. Talley, T.R. Huser, R. Bogomolni, J.Z. Zhang, Unique gold nanoparticle aggregates as a highly active surface-enhanced raman scattering substrate, J. Phys. Chem. B 108 (2004) 19191–19197, https://doi.org/10.1021/jp048430p.

[10] J.C. Fraire, L.A. Pérez, E.A. Coronado, Cluster size effects in the surface-enhanced raman scattering response of ag and au nanoparticle aggregates: experimental and theoretical insight, J. Phys. Chem. C 117 (2013) 23090–23107, https://doi.org/10.1021/jp3123709.

[11] F. Tian, F. Bonnier, A. Casey, A.E. Shanahan, H.J. Byrne, Surface enhanced Raman scattering with gold nanoparticles: effect of particle shape, Anal. Methods 6 (2014) 9116–9123, https://doi.org/10.1039/c4ay02112f.

[12] M. Fan, G.F.S. Andrade, A.G. Brolo, A review on the fabrication of substrates for surface enhanced Raman spectroscopy and their applications in analytical chemistry, Anal. Chim. Acta 693 (2011) 7–25, https://doi.org/10.1016/j.aca.2011.03.002.

[13] M. Oćwieja, D. Lupa, Z. Adamczyk, Gold nanoparticle layers on polystyrene microspheres of controlled structure and electrokinetic properties, Langmuir. 34 (2018) 8489–8498, https://doi.org/10.1021/acs.langmuir.8b01491.

[14] O. Péron, E. Rinnert, T. Toury, M. Lamy De La Chapelle, C. Compère, Quantitative SERS sensors for environmental analysis of naphthalene, Analyst. 136 (2011) 1018–1022, https://doi.org/10.1039/c0an00797h.

[15] A. Yamaguchi, T. Fukuoka, R. Takahashi, R. Hara, Y. Utsumi, Dielectrophoresis-enabled surface enhanced Raman scattering on gold-decorated polystyrene microparticle in micro-optofluidic devices for high-sensitive detection, Sensors Actuators B Chem. 230 (2016) 94–100, https://doi.org/10.1016/j.snb.2016.02.023.

[16] A.B. Serrano-Montes, J. Langer, M. Henriksen-Lacey, D. Jimenez De Aberasturi, D.M. Solís, J.M. Taboada, F. Obelleiro, K. Sentosun, S. Bals, A. Bekdemir, F. Stellacci, L.M. Liz-Marzán, Gold nanostar-coated polystyrene beads as multifunctional nanoprobes for SERS bioimaging, J. Phys. Chem. C 120 (2016) 20860–20868, https://doi.org/10.1021/acs.jpcc.6b02282.

[17] G. Ren, M. Shang, H. Zou, W. Wang, Fe3O4@SiO2-SO3H@PPy@Au spheres: fabrication, characterization and application in SERS, Mater. Chem. Phys. 173 (2016) 333–339, https://doi.org/10.1016/j.matchemphys.2016.02.020.

[18] M. Kanahara, H. Satoh, T. Higuchi, A. Takahara, H. Jinnai, K. Harano, S. Okada, E. Nakamura, Y. Matsuo, H. Yabu, Fabrication of NIR-excitable SERS-active composite particles composed of densely packed au nanoparticles on polymer microparticles, Part. Part. Syst. Charact. 32 (2015) 441–447, https://doi.org/10.1002/ppsc.201400191.

[19] P. Pinheiro, S. Fateixa, T. Trindade, SERS detection of penicillin G using magnetite decorated with gold nanoparticles, Magnetochemistry. 3 (2017) 32, https://doi.org/10.3390/magnetochemistry3040032.

[20] P. Quaresma, I. Osório, G. Dória, P.A. Carvalho, A. Pereira, J. Langer, J.P. Araújo, I. Pastoriza-Santos, L.M. Liz-Marzán, R. Franco, P.V. Baptista, E. Pereira, Star-shaped magnetite@gold nanoparticles for protein magnetic separation and SERS detection, RSC Adv. 4 (2014) 3659–3667, https://doi.org/10.1039/c3ra46762g.

[21] J. Du, J. Xu, Z. Sun, C. Jing, Au nanoparticles grafted on Fe3O4 as effective SERS substrates for label-free detection of the 16 EPA priority polycyclic aromatic hydrocarbons, Anal. Chim. Acta 915 (2016) 81–89, https://doi.org/10.1016/j.aca.2016.02.009.

[22] D. Cassano, M. Santi, V. Cappello, S. Luin, G. Signore, V. Voliani, Biodegradable passion fruit-like Nano-architectures as carriers for cisplatin prodrug, Part. Part. Syst. Charact. 33 (2016) 818–824, https://doi.org/10.1002/ppsc.201600175.

[23] J.F. Li, Y.J. Zhang, S.Y. Ding, R. Panneerselvam, Z.Q. Tian, Core-shell nanoparticle-enhanced raman spectroscopy, Chem. Rev. 117 (2017) 5002–5069, https://doi.org/10.1021/acs.chemrev.6b00596.

[24] S.L. Westcott, S.J. Oldenburg, T.R. Lee, N.J. Halas, Halas_Langmuir_1998(1), 7463, (1998), pp. 1–6 papers2://publication/uuid/324BB545-9E55-469C-9C27-4CF9A46142EE.

[25] C. Graf, S. Dembski, A. Hofmann, E. Rühl, A general method for the controlled embedding of nanoparticles in silica colloids, Langmuir. 22 (2006) 5604–5610, https://doi.org/10.1021/la060136w.

[26] A. Le Beulze, S. Gomez-Graña, H. Gehan, S. Mornet, S. Ravaine, M. Correa-Duarte, L. Guerrini, R.A. Alvarez-Puebla, E. Duguet, E. Pertreux, A. Crut, P. Maioli, F. Vallée, N. Del Fatti, O. Ersen, M. Treguer-Delapierre, Robust raspberry-like metallo-dielectric nanoclusters of critical sizes as SERS substrates, Nanoscale. 9 (2017) 5725–5736, https://doi.org/10.1039/c7nr00969k.

[27] V.G. Pol, A. Gedanken, J. Calderon-Moreno, Deposition of gold nanoparticles on silica spheres: a sonochemical approach, Chem. Mater. 15 (2003) 1111–1118, https://doi.org/10.1021/cm021013+.

[28] S.J. Oldenburg, S.L. Westcott, R.D. Averitt, N.J. Halas, Surface enhanced Raman scattering in the near infrared using metal nanoshell substrates, J. Chem. Phys. 111 (1999) 4729–4735, https://doi.org/10.1063/1.479235.

[29] B. Sadtler, A. Wei, Spherical ensembles of gold nanoparticles on silica: electrostatic and size effects, Chem. Commun. 2 (2002) 1604–1605, https://doi.org/10.1039/b204760h.

[30] P. Khurana, S. Thatai, P. Wang, P. Lihitkar, L. Zhang, Y. Fang, S.K. Kulkarni, Speckled SiO2@Au core-shell particles as surface enhanced Raman scattering probes, Plasmonics. 8 (2013) 185–191, https://doi.org/10.1007/s11468-012-9374-0.

[31] A. Baliś, S. Zapotoczny, Tailored synthesis of Core-Shell mesoporous silica particles—optimization of dye sorption properties, Nanomaterials. 8 (2018) 230, https://doi.org/10.3390/nano8040230.

[32] T. Niidome, K. Nakashima, H. Takahashi, Y. Niidome, Preparation of primary amine-modified gold nanoparticles and their transfection ability into cultivated cells, Chem. Commun. 10 (2004) 1978–1979, https://doi.org/10.1039/b406189f.

[33] M. Oćwieja, J. Maciejewska-Prończuk, Z. Adamczyk, M. Roman, Formation of positively charged gold nanoparticle monolayers on silica sensors, J. Colloid Interface Sci. 501 (2017) 192–201, https://doi.org/10.1016/j.jcis.2017.04.038.

[34] F. Barahona, O. Geiss, P. Urbán, I. Ojea-Jimenez, D. Gilliland, J. Barrero-Moreno, Simultaneous determination of size and quantification of silica nanoparticles by asymmetric flow field-flow fractionation coupled to ICPMS using silica nanoparticles standards, Anal. Chem. 87 (2015) 3039–3047, https://doi.org/10.1021/ac504698j.

[35] Z. Adamczyk, K. Sadlej, E. Wajnryb, M. Nattich, M.L. Ekiel-Jezewska, J. Bławzdziewicz, Streaming potential studies of colloid, polyelectrolyte and protein deposition, Adv. Colloid Interf. Sci. 153 (2010) 1–29, https://doi.org/10.1016/j.cis.2009.09.004.

[36] M. Ujihara, N.M. Dang, T. Imae, Surface-enhanced resonance raman scattering of rhodamine 6G in dispersions and on films of confeito-like Au nanoparticles, Sensors (Switzerland). 17 (2017), https://doi.org/10.3390/s17112563.

[37] E.O. Ganbold, J.H. Park, U. Dembereldorj, K.S. Ock, S.W. Joo, Charge-dependent adsorption of rhodamine 6G on gold nanoparticle surfaces: fluorescence and Raman study, J. Raman Spectrosc. 42 (2011) 1614–1619, https://doi.org/10.1002/jrs.2907.

[38] C. Ruan, W. Wang, B. Gu, Surface-enhanced Raman scattering for perchlorate detection using cystamine-modified gold nanoparticles, Anal. Chim. Acta 567 (2006) 114–120, https://doi.org/10.1016/j.aca.2006.01.097.

[39] I.L. Arbeloa, P.R. Ojeda, Molecular forms of rhodamine B, Chem. Phys. Lett. 79 (1981) 347–350, https://doi.org/10.1016/0009-2614(81)80219-9.

[40] F. Castillo, E. De La Rosa, E. Pérez, Gold aggregates on silica templates and decorated silica arrays for SERS applications, Eur. Phys. J. D. 63 (2011) 301–306, https://doi.org/10.1140/epjd/e2011-10605-7.

[41] W. Wang, Z. Meng, Q. Zhang, X. Jia, K. Xi, Synthesis of stable Au-SiO 2 composite nanospheres with good catalytic activity and SERS effect, J. Colloid Interface Sci. 418 (2014) 1–7, https://doi.org/10.1016/j.jcis.2013.11.043.

[42] F. Wang, Y. Tang, B. Zhang, B. Chen, Y. Wang, Preparation of novel magnetic hollow mesoporous silica microspheres and their efficient adsorption, J. Colloid Interface Sci. 386 (2012) 129–134, https://doi.org/10.1016/j.jcis.2012.06.088.

[43] X. Gao, J. He, L. Deng, H. Cao, Synthesis and characterization of functionalized rhodamine B-doped silica nanoparticles, Opt. Mater. (Amst). 31 (2009) 1715–1719, https://doi.org/10.1016/j.optmat.2009.05.004.